CrossMark

Synthesis and characterization of magnetite/hydroxyapatite tubes using natural template for biomedical applications

M SNEHA, N MEENAKSHI SUNDARAM* and A KANDASWAMY

Department of Biomedical Engineering, PSG College of Technology, Coimbatore 641004, Tamil Nadu, India

Abstract. Inorganic nanotubes have attracted much attention during the last few decades for its potential applications in the field of regenerative medicine and controlled drug delivery. In the present work, we have designed and synthesized magnetite hydroxyapatite micro and nanotubes. The first step is the formation of magnetite (Fe_3O_4) tubes on natural template followed by hydroxyapatite (HAp) bioceramic coated on the Fe_3O_4 tubes. HAp improves the biocompatibility and stability of the prepared tubes. Sintering at 900°C improves the crystalline stability of nanotubes and removes the natural template. X-ray diffraction, N_2 adsorption–desorption studies (BET), thermogravimetric analysis, differential scanning calorimetry, optical micrographs, field emission scanning electron microscope and transmission electron microscope studies were carried out to confirm the structural and morphological analysis of prepared magnetic tubular structure.

1. Introduction

Nanotechnology has become a promising and multifaceted platform for the discovery of novel materials with improved properties and applications in cancer treatment. Nanomaterials have extremely good potential for early detection, diagnosis and treatment of cancer [1]. The advantages of nanoparticle-based drug delivery system include reduced side effects, longer circular time and improved pharmacokinetics [2–4]. Cancer is a most dreadful disease and is still not easily treated by conventional therapies. Hyperthermia is the delivery of heat to the tumour cells. It is used in combination with other modalities of treatment, such as radiotherapy, chemotherapy and surgery [5].

When superparamagnetic nanoparticles are subjected to an AC magnetic field, it shows extraordinary heating effects due to the magnetization reversal process of the particles (such as Neel and Brownian relaxation process). In magnetically mediated hyperthermia, the magnetic nanoparticles are targeted towards the tumour site and heated using an external alternating magnetic field in the range of 0–15 kA m^{-1} at a frequency of 100 kHz [6,7]. Superparamagnetic iron oxide nanoparticles, especially magnetite phase (Fe_3O_4), are widely used for imaging and therapeutic applications as they are capable of non-invasive detection and treatment of tumours. When they are used in conjugation or loaded with tumour-specific targeting ligands, these nanoparticles have the ability to deliver the anti-cancer drugs specifically to tumours and, therefore, the side effects can be minimized on the normal cells [8–10]. The magnetic nanotubes must be coated with a biocompatible material to improve its stability and biocompatibility [11]. The calcium phosphate-based bioceramics such as hydroxyapatite (HAp) plays a vital role in biomedical applications due to its excellent properties like bioactivity, osteoconductivity and biocompatibility [12]. HAp is predominantly used in nanomedicine for applications in bone reconstruction and cancer treatment [13]. The effect of magnetic field on the orientation of HAp nanocrystals in a magnetic field under physiological conditions shows magnetic control over the biomaterials response [14].

Synthesis of nanotubes from inorganic materials has also attracted attention due to its unique applications in the areas such as sensing, catalysis and electronics [15]. The double end opened tubular nanostructures are ideal for drug loading and delivery applications in a controlled mechanism. Nanotubes have been synthesized from a variety of inorganic materials such as SiO_2 [16], TiO_2 [17], Al_2O_3 [18], CdSe [19], ZnS [20], Au [21], Co and Fe [22].

According to Chandanshive *et al* [23] HAp nanotubes synthesis involves a sol-gel process under neutral conditions in the presence of a sacrificial anodic alumina template. The diameter of the resulting tubes was in the range of 14–350 nm [23]. Lee *et al* [24] synthesized iron oxide nanotubes by prolonged sintering of iron oxide nanoparticles during chemical vapour condensation at 800°C for 6 h [24]. Singh *et al* [11] prepared poly (caprolactone)-based magnetic hydroxyapatite nanotubes (MHAnt). A hollow tube of HA-MNPs was created, in which HA formed an outer shell and most of the MNPs lined the inner shell surface [11].

In this work, we have developed HAp-coated Fe_3O_4 nanotubes by Ceiba pentandra as templates. The coating of HAp onto the Fe_3O_4 core structure has been confirmed by field

*Author for correspondence (nmsundaram75@gmail.com)

emission scanning electron microscope (FE-SEM), transmission electron microscope (TEM) and selected area electron diffraction (SAED) patterns. So, cancer drug-loaded HAp-coated magnetite tubular structure is an ideal applicant for magnetic hyperthermia, especially in bone cancer (osteosarcoma) treatment. So far, there is no work on natural template HAp-coated magnetite (Fe_3O_4) tubular structure.

2. Materials and methods

2.1 *Kapok fibre*

Kapok fibres (figure 1) were isolated from its seeds and washed with distilled water and ethanol to remove the impurities.

2.2 *Preparation of iron oxide tubular structure*

Kapok fibres were immersed in ferric chloride solution ($0.25 \, mol \, l^{-1}$) for 1 h. Ferrous chloride solution ($0.125 \, mol \, l^{-1}$) was then added to the above solution under constant stirring for 1 h. pH was adjusted to 12 by using sodium hydroxide ($1 \, mol \, l^{-1}$). The entire solution was maintained at 70°C for 1 h. It was washed several times with distilled water to remove any impurities present and finally dried.

2.3 *Preparation of HAp tubular structure*

Kapok fibres were immersed in calcium nitrate solution ($1 \, mol \, l^{-1}$) for 1 h. Diammonium hydrogen phosphate solution ($0.6 \, mol \, l^{-1}$) was then added to the above solution under constant stirring for 1 h. pH was adjusted to 10 by using ammonia solution. The entire solution was maintained at 70°C for 1 h. It was washed several times with distilled water to remove any impurities present and finally dried.

Figure 1. Kapok fibres.

2.4 *Preparation of HAp-coated iron oxide tubular structure*

The Fe_3O_4 loaded fibres were dispersed in calcium nitrate solution ($1 \, mol \, l^{-1}$) under stirring for 1 h. Diammonium hydrogen phosphate ($0.6 \, mol \, l^{-1}$) was added to the above solution under stirring for 1 h. Ammonia solution was used to adjust the pH value between 8 and 10. The solution was kept for ageing for 24 h and washed with distilled water. It was then dried at 70°C overnight. The dried sample was sintered at 900°C for 2 h and stored in an airtight container for further analysis.

2.5 *Preparation of iron oxide coated on HAp tubular structure*

The HAp loaded fibres were dispersed in ferric chloride solution ($0.25 \, mol \, l^{-1}$) under stirring for 1 h. Ferrous chloride solution ($0.125 \, mol \, l^{-1}$) was added to the above solution under stirring for 1 h. Sodium hydroxide solution was used to adjust the pH to 12. The solution was kept for ageing for 24 h and washed with distilled water. It was then dried at 70°C overnight. The dried sample was sintered at 900°C for 2 h and stored in an airtight container for further analysis.

3. Characterization

3.1 *Powder X-ray diffractometer*

Figure 2 shows the X-ray diffraction (XRD) patterns of the (a) pure iron oxide, (b) pure HAp, (c) iron oxide-coated HAp and (d) HAp-coated iron oxide. The characteristic peaks in the pattern of iron oxide agree well the standard
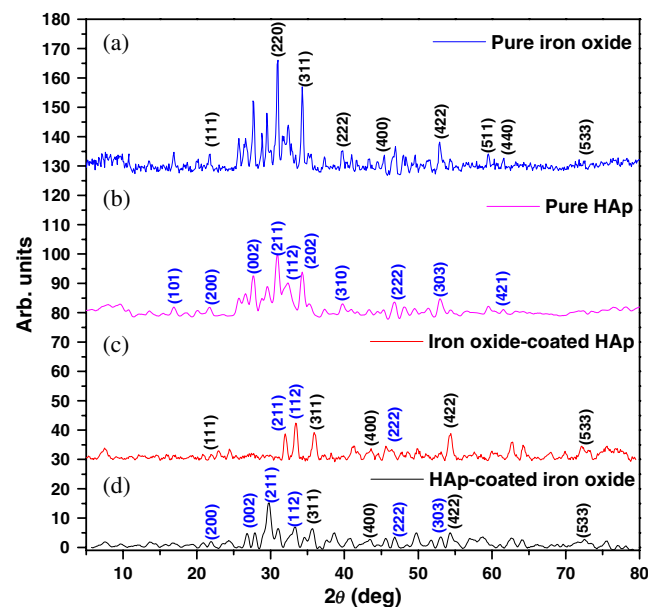

Figure 2. X-ray diffraction patterns of the (a) pure iron oxide, (b) pure HAp, (c) iron oxide-coated HAp and (d) HAp-coated iron oxide.

JCPDS pattern of (19-0629). The XRD patterns of the powder obtained were in good agreement with the XRD patterns of an HAp standard available in JCPDS (09-0432). The HAp coated with iron oxide exhibits a mixed phase of both HAp and iron oxide and vice versa.
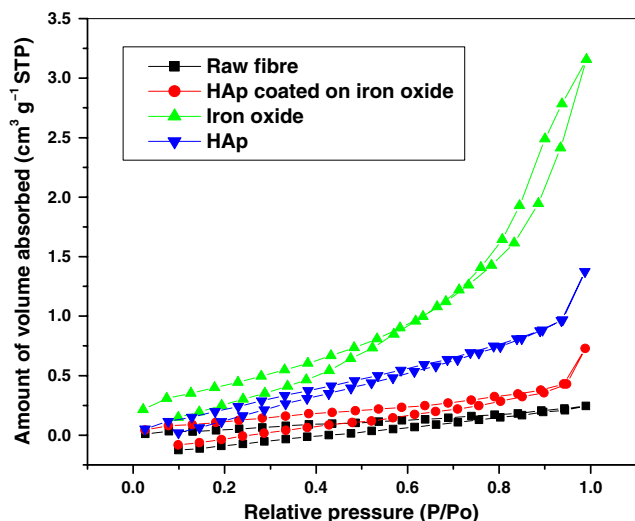
Figure 3. N_2 adsorption–desorption studies of raw fibre, iron oxide, HAp and HAp coated on iron oxide.

Table 1. Surface characteristics of prepared samples.

	Surface area (m^2 g^{-1})	Pore volume (cc g^{-1})	Pore size (nm)
HAp	5.185	0.006159	7.447
Iron oxide	75.082	0.1839	6.231
HAp-coated iron oxide	6.623	0.0126	6.318
Raw fibre	9.697	0.008953	6.330

3.2 *N_2 adsorption–desorption studies (BET)*

The nitrogen adsorption and desorption isotherm of synthesized HAp-coated iron oxide is shown in figure 3. In this study, we have observed that the synthesized material has less surface area and irregular isotherm curve. Small surface area indicates that the material has a large amount of aggregation during the calcinations process. The surface area, pore volume, pore size are mentioned in table 1.

### 3.3 *Thermogravimetric analysis*

Thermal stability of raw kapok fibres and iron oxide/HAp fibres was obtained by using TA Q500 with a heating rate of 20°C min^{-1}, from 100 to 600°C in a nitrogen atmosphere. Thermogravimetric analysis (TGA) was used to measure the weight loss of fibres as a function of rising temperature.

In figure 4a, the first stage of weight loss was observed between 100 and 269°C, which corresponds to the release of moisture content from the fibre. The second stage of weight loss occurred between the temperature 270 and 361°C, which is due to the degradation of lignin and hemicellulose. The third stage of weight loss occurred between the temperature 362 and 510°C, due to degradation of cellulose and other cellulosic matters from the fibre.

In figure 4b (before sintering), the first stage of weight loss was observed between 100 and 160°C, which is due to the vapourization of adsorbed water. The second stage of weight loss occurred between the temperature 161 and 311°C, due to crystallization of HAp. The third stage of weight loss occurred between the temperature 312 and 761°C, due to the breakage of CO_3^{2-} and HPO_4.

3.4 *Differential scanning calorimetry*

Kapok fibre shows a small exothermic peak at 340°C and minor endothermic peak around 370°C (figure 5a). In
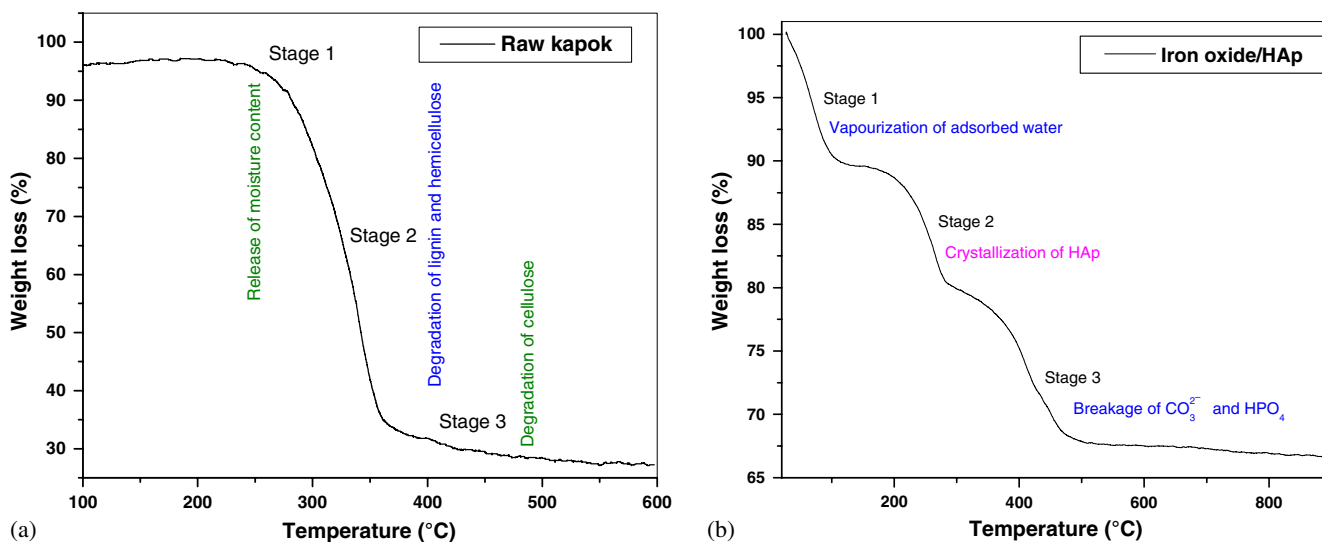
Figure 4. (**a**) TGA of raw kapok fibre and (**b**) TGA of iron oxide/HAp.

differential scanning calorimetry (DSC), a strong endothermic peak was observed between 95 and 100°C. This is due to the removal of the solvent molecule. Two slight endothermic peaks were observed at 290 and 430°C. The second peak is due to crystallization process. Another slight endothermic peak was observed at 520°C. This is due to magnetite phase crystallization (figure 5b).

3.5 *Optical micrographs*

Figure 6a presents optical microscope images of raw kapok fibres and its cross-sectional image. In our experiment,

we coated iron oxide nanoparticle on kapok fibre. The microscope image reveals the fine structural features of the material surfaces. The iron oxide nanoparticles have coated 70% on the fibre template and nanoparticle aggregation on the sides of the tubes can be seen from figure 6b. The nanoparticles are deposited only on the outer surface of the fibre template; surprisingly, the nanoparticles did not spread through the surfaces inside the fibre. Uniform deposition of HAp nanoparticles on the fibre template can be seen from figure 6c. The cross-sectional view of HAp showed a tubular structure with nanometre-sized diameters. It has unique properties that can be exploited in the
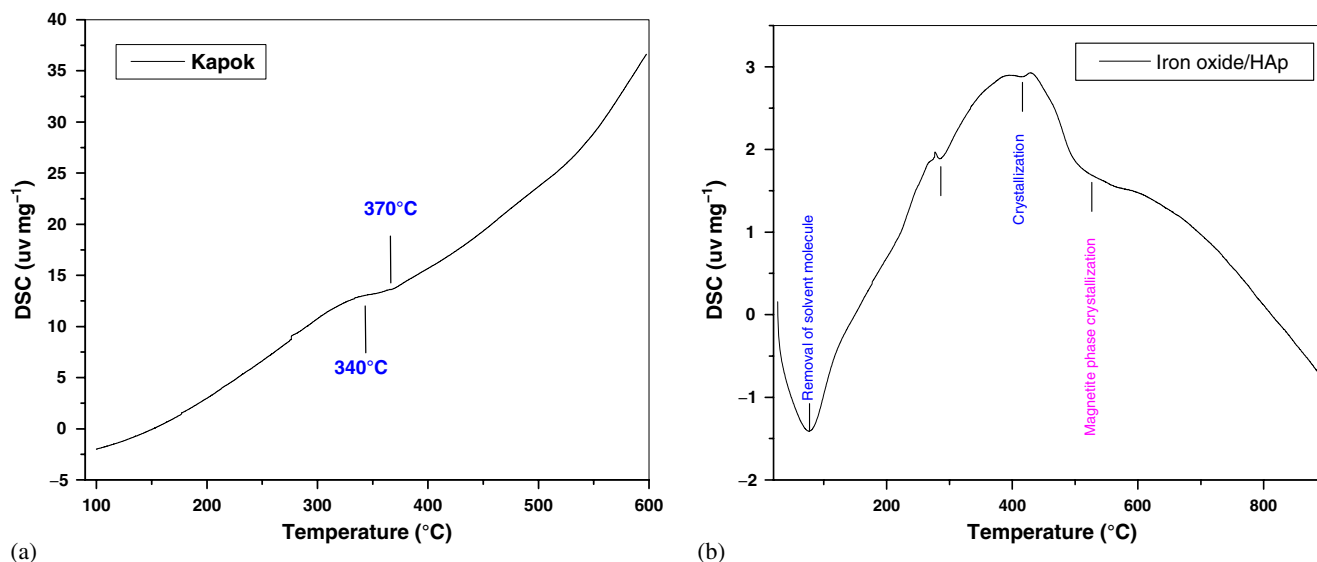

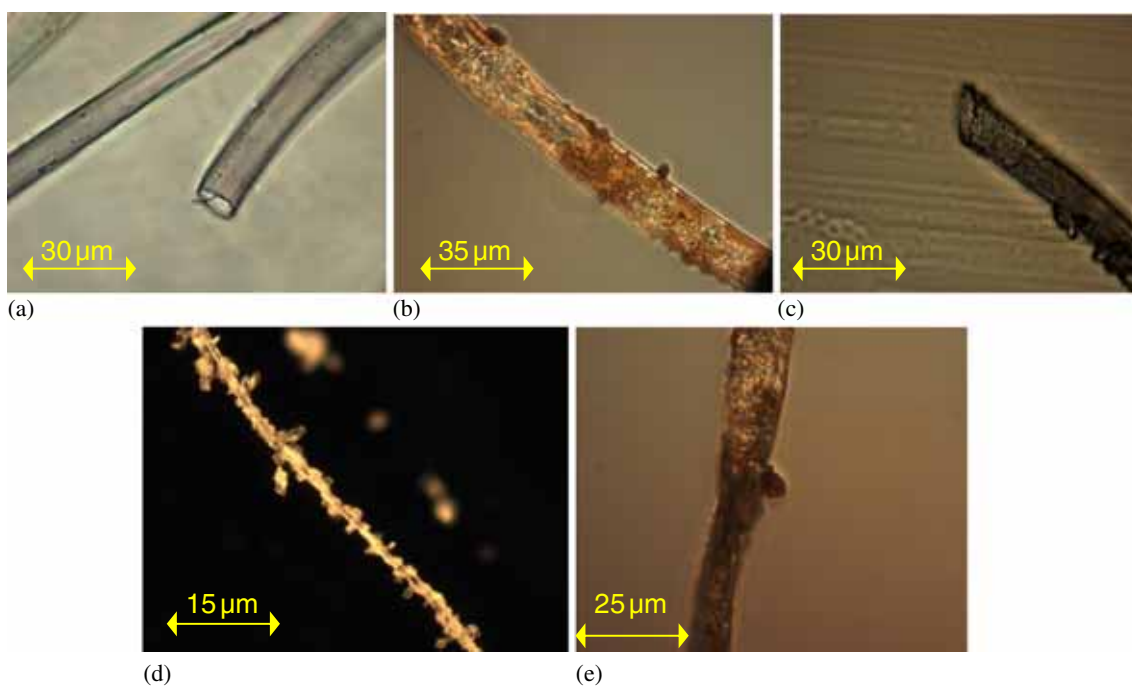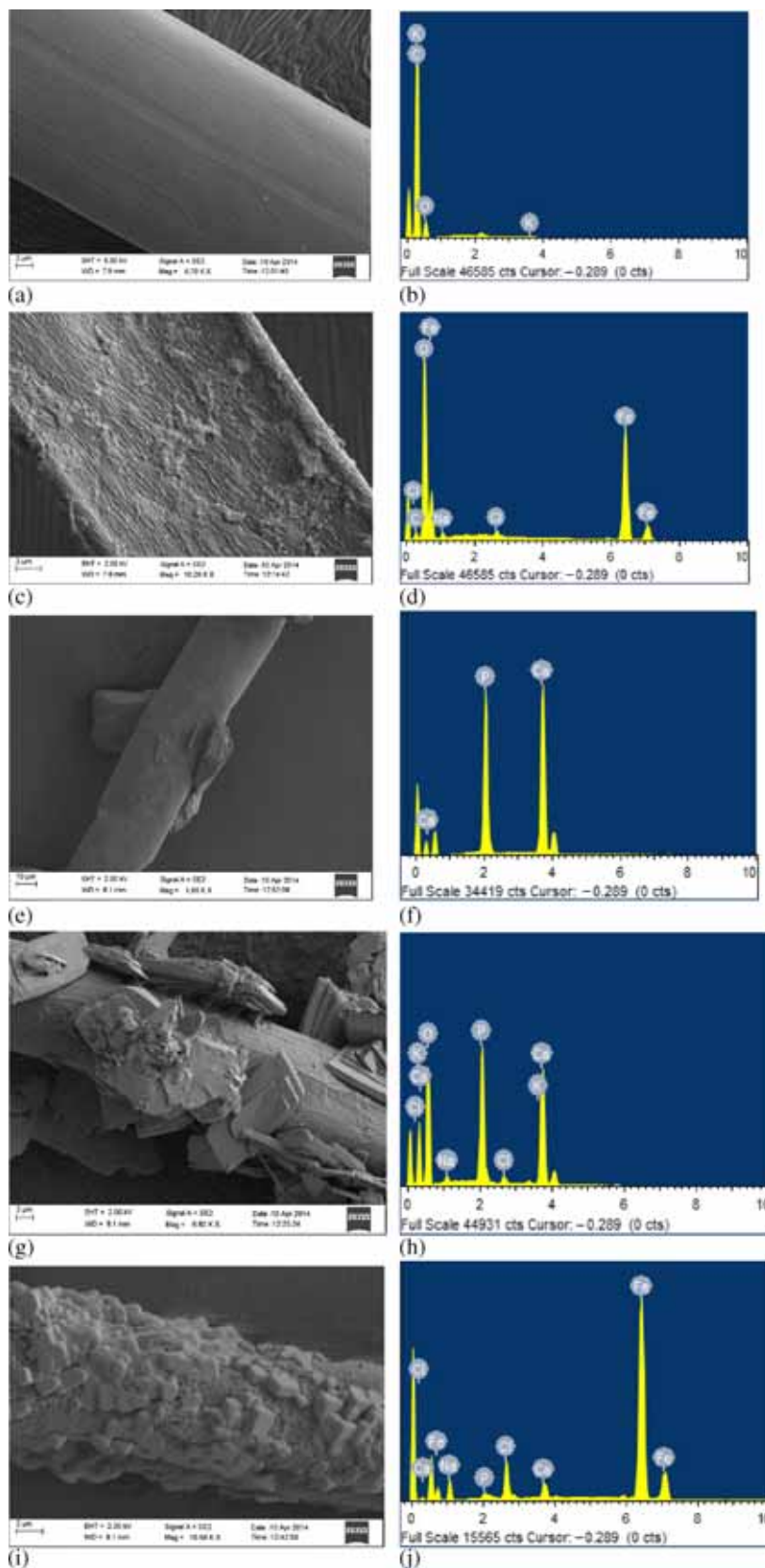**Figure 5.** (**a**) DSC of raw kapok fibre and (**b**) iron oxide/HAp.

Figure 6. Optical micrograph of (**a**) kapok fibre, (**b**) iron oxide nanoparticle, (**c**) hydroxyapatite nanoparticles, (**d**) HAp coating on iron oxide tube and (**e**) iron oxide coating on HAp tube.

Figure 7. (**a**) FE-SEM image, (**b**) EDAX of raw kapok fibre, (**c**, **d**) iron oxide nanoparticles coated on kapok fibre and its EDAX, (**e**, **f**) hydroxyapatite nanoparticles coated on kapok fibre and its EDAX, (**g**, **h**) hydroxyapatite nanoparticles coated on iron oxide-kapok fibre and its EDAX and (**i**, **j**) iron oxide nanoparticles coated on hydroxyapatite-kapok fibre and its EDAX.

diagnosis and treatment of cancer. In figure 6d, the coating of HAp nanoparticles on iron oxide-kapok template can be visualized clearly under the optical microscope. The HAp is deposited uniformly on the template, and this condition is highly suited for hyperthermia and drug delivery apllications. The deposition of iron oxide nanoparticles on HAp-kapok template can be seen clearly in figure 6e. The smooth and ordered coating on nanoparticles is essential in biomedical applications.

3.6 *FE-SEM (with template)*

A silky appearance and smooth surface can be seen for raw kapok fibre in figure 7a. By the microscope observation, kapok fibres are transparent with characteristic air bubbles in the lumen. Kapok fibres are 10–35 mm long, with a diameter of 20–43 μm. The EDAX analysis shows that the pure kapok fibre consists of carbon and oxygen due to its pure cellulose structure. In figure 7c, the deposition of iron
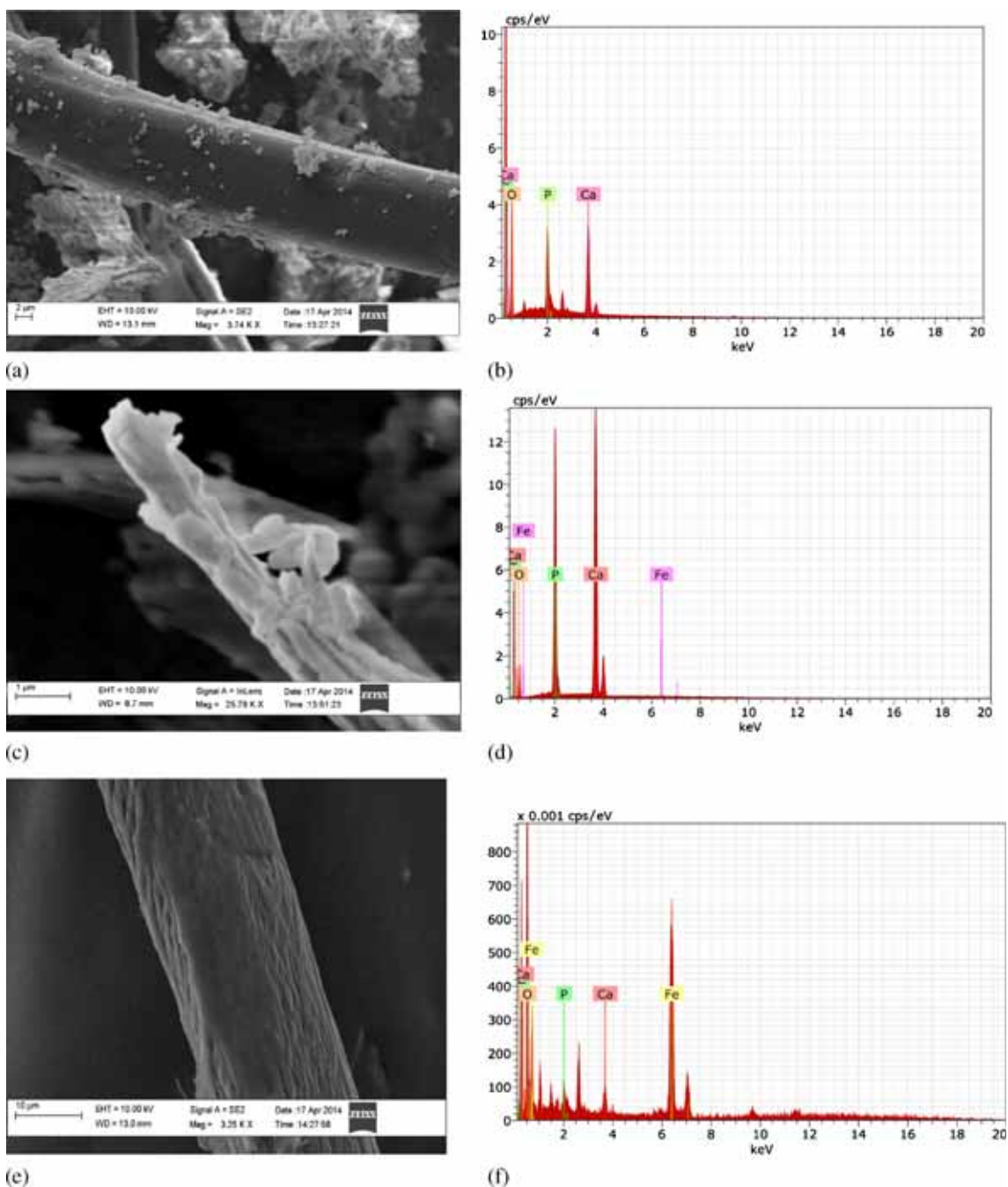
Figure 8. (**a**, **b**) FE-SEM images of HAp tubes and its EDAX, (**c**, **d**) HAp nanoparticles coated on iron oxide and its EDAX and (**e**, **f**) iron oxide nanoparticles coated on HAp and its EDAX.

oxide nanoparticles on kapok fibre can be visualized under FE-SEM. The air entrapment inside the fibre disappeared after coating with iron oxide nanoparticle. The structure became completely flattened. The overall tubular structure was retained and unbroken. The surface of the fibres was also rougher. The uniform coating of HAp nanoparticles on the fibre surface can be visualized and in addition to the coating, HAp aggregates also attached to the surface which is seen in figure 7e. This may be due to longer exposure of nanoparticles to the template. The HAp is well coated on iron oxide-kapok fibre, as seen in figure 7g. In figure 7i, a continous coating of iron oxide nanoparticles on HAp-kapok fibre can be seen under FE-SEM analysis.

Calcination: These samples were calcined to remove the kapok fibre templates. The calcination temperature for iron oxide and HAp tubes is 900°C for 2 h.

3.7 *FE-SEM (after removal of template)*

The micromorphology and surface analysis of the prepared sample are carried out by field emission scanning electron microscope, which is shown in figure 8. Figure 8a shows the pure HAp nanotubes formed on the kapok fibre. It has an uniform and smooth surface. Several millimetres long tubular structures are formed even after the removal of the kapok template. The EDAX analysis shows that the formed composition was calcium-rich HAp with a Ca/P ratio of 1.7928. Figure 8c shows the HAp-coated Fe_3O_4 nanotubular structure. Several tubular-like structures are observed after the sintering process. The EDAX analysis exihibits the presence of Fe_3O_4 in the inner core and stochiometric formation of HAp with Ca/P ratio of 1.682 on the outer core. Since Fe_3O_4 is well buried inside, poor iron signals are identified. Iron oxide nanoparticles coated on HAp is shown in figure 8e.
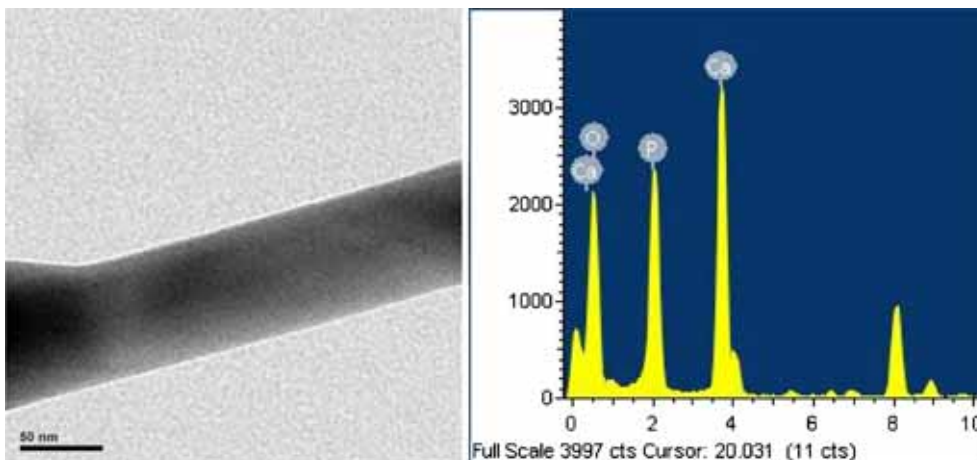
3.8 *Transmission electron microscope*

3.8a *Iron oxide tubular structure*: Figure 9 represents the TEM image of synthesized magnetite tubular structure, with the length of 100–110 nm.
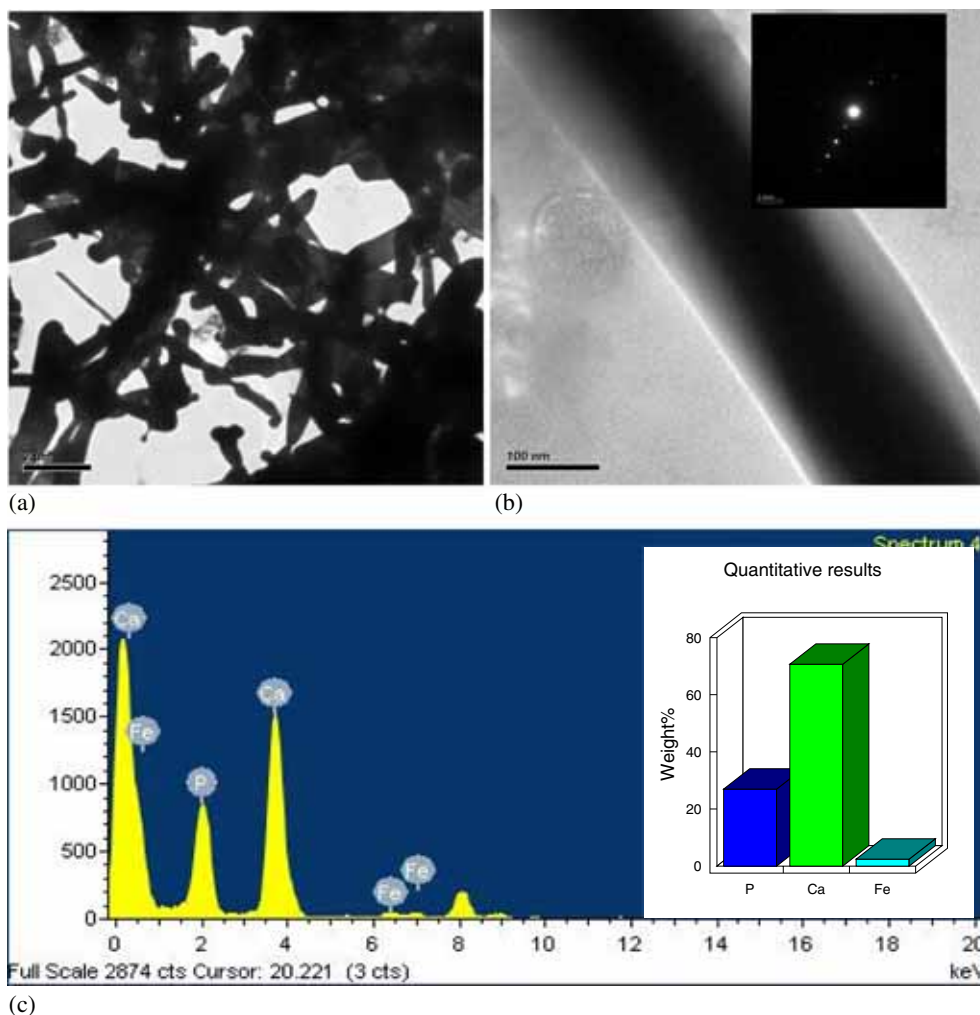
3.8b *HAp tubular structure*: The TEM image of HAp tubular structure is shown in figure 10, in which the
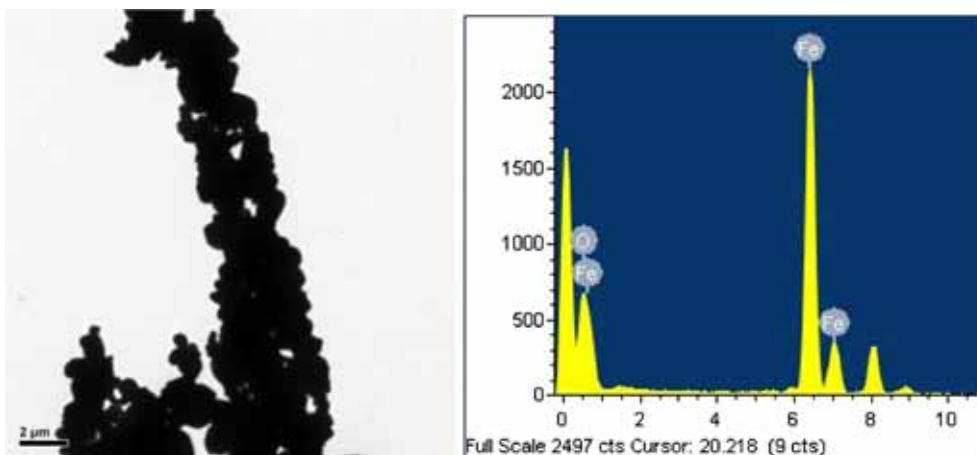
Figure 9. Iron oxide tubular structure.

Figure 10. HAp tubular structure.

Figure 11. (**a**, **b**) TEM images of HAp nanoparticles coated on iron oxide tubular structure and (**c**) EDAX.

tubular-like structure can be seen clearly, with the length of 70–80 nm.

3.8c *HAp-coated iron oxide tubular structure*: The TEM analysis of HAp-coated iron oxide nanotubes templated by kapok nanofibre shows that the tubular-like structure consists of HAp and iron oxide. The further magnification of the surface shows nanotubular-like structure (figure 11). The formed tubular structures have iron oxide core as an inner layer and HAp as an outer layer. These nanotubular composite structures have an inner diameter of 300 nm and an outer diameter of 500 nm. The SAED pattern shown in figure 2b exhibits the presence of Fe_3O_4 and HAp structure.

4. Conclusion

In conclusion, HAp-coated magnetite tubular structure developed through a simple natural template-mediated method revealed that the obtained nanotubes are composed of HAp and Fe_3O_4 (by FE-SEM and TEM analyses). This magnetic tubular structure can be effectively used for magnetic hyperthermia treatment with suitable drug-loading strategy.

References

[1] Weibo Cai and Xiaoyuan Chen 2007 *Small* **3** 1840

[2] Davis M E, Chen Z G and Shin D M 2008 *Nat. Rev. Drug Discov.* **7** 771

[3] Zhang L, Gu F X, Chan J M, Wang A Z, Langer R S and Farokhzad O C 2008 *Clin. Pharmacol. Ther.* **83** 761

[4] Peer D, Karp J M, Hong S, Farokhzad O C, Margalit R and Langer R 2007 *Nat. Nanotechnol.* **2** 751

[5] Gianfranco Baronzio, Gurdev Parmar, Marco Ballerini, Andras Szasz, Miriam Baronzio and Valter Cassutti 2014 *J. Integr. Oncol.* **3** 115

[6] Rudolf Hergt, Silvio Dutz, Robert Müller and Matthias Zeisberger 2006 *J. Phys.: Condens. Matter* **18** S2919

[7] Sophie Laurent, Silvio Dutz, Urs O Häfeli and Morteza Mahmoudi 2011 *Adv. Colloid Interface Sci.* **166** 8

[8] McCarthy J R, Kelly K A, Sun E Y and Weissleder R 2007 *Nanomedicine* **2** 153

[9] Ajay Kumar Gupta and Mona Gupta 2005 *Biomaterials* **26** 3995

[10] Nasongkla N, Bey E, Ren J, Ai H, Khemtong C, Guthi J S, Chin S F, Sherry A D, Boothman D A and Gao J 2006 *Nano Lett.* **6** 2427

[11] Rajendra K Singh, Ahmed M El-Fiqi, Kapil D Patel and Hae-Won Kim 2012 *Mater. Lett.* **75** 130

[12] Anee Kuriakose T, Narayana Kalkura S, Palanichamy M, Arivuoli D, Karsten Dierks, Bocelli G and Betzel C 2004 *J. Cryst. Growth* **263** 517

[13] María Vallet-Regi and Eduardo Ruiz-Hernández 2011 *Adv. Mater.* **23** 5177

[14] Meenakshi Sundaram N, Girija E K, Ashok M, Yokogawa Y and Kalkura S N 2006 *Mater. Lett.* **60** 761

[15] Yujie Xiong, Brian T, Mayers and Younan Xia 2005 *Chem. Commun.* **40** 5013

[16] Hidenori Nakamura and Yasushi Matsui 1995 *J. Am. Chem. Soc.* **117** 2651

[17] Patrick Hoyer 1996 *Langmuir* **12** 1411

[18] Lin Pu, Ximao Bao, Jianping Zou and Duan Feng 2001 *Angew. Chem. Int. Ed* **40** 1490

[19] Rao C N R, Govindaraj A, Leonard Deepak F, Gunari N A and Manashi Nath 2001 *Appl. Phys. Lett.* **78** 1853

[20] Dloczik1 L, Engelhardt R, Ernst K, Fiechter S, Sieber I and Könenkamp R 2001 *Appl. Phys. Lett.* **78** 3687

[21] John C Hulteen, Kshama B Jirage and Charles R Martin 1998 *J. Am. Chem. Soc.* **120** 6603

[22] Tourillon G, Pontonnier L, Levy J P and Langlais V 2000 *Electrochem. Solid-State Lett.* **3** 20

[23] Balasaheb B Chandanshive, Priyanka Raib, Andre L Rossic, Ovidiu Ersenc and Deepa Khushalan 2013 *Mater. Sci. Eng. C* **33** 2981

[24] Chang-Woo Lee, Kyoung-No Lee and Jai-Sung Lee 2009 *Mater. Lett.* **63** 2607